

## Singular Jets and Bubbles in Drop Impact

Denis Bartolo,<sup>1,\*</sup> Christophe Josserand,<sup>2,†</sup> and Daniel Bonn<sup>1,3,‡</sup>

<sup>1</sup>Laboratoire de Physique Statistique de l'ENS, 24 Rue Lhomond, 75231 Paris Cédex 05, France

<sup>2</sup>Laboratoire de Modélisation en Mécanique, CNRS-UMR 7606, Case 162, 4 place Jussieu, 75252 Paris Cédex 05, France

<sup>3</sup>van der Waals-Zeeman Institute, University of Amsterdam, Valckenierstraat 65, 1018 XE Amsterdam, The Netherlands

(Received 21 November 2005; published 27 March 2006)

We show that when water droplets gently impact on a hydrophobic surface, the droplet shoots out a violent jet, the velocity of which can be up to 40 times the drop impact speed. As a function of the impact velocity, two different hydrodynamic singularities are found that correspond to the collapse of the air cavity formed by the deformation of the drop at impact. It is the collapse that subsequently leads to the jet formation. We show that the divergence of the jet velocity can be understood using simple scaling arguments. In addition, we find that very large air bubbles can remain trapped in the drops. The surprising occurrence of the bubbles for low-speed impact is connected with the nature of the singularities, and can have important consequences for drop deposition, e.g., in ink-jet printing.

DOI: 10.1103/PhysRevLett.96.124501

PACS numbers: 47.55.D-, 47.20.Cq, 47.20.Dr

Droplets impacting on solid surfaces have fascinated scientists and even artists ever since the first pictures became available [1]. From a practical point of view, the control of the impact dynamics is of prime importance: droplet deposition is a key factor in many industrial processes. Pertinent examples are ink-jet printing [2], sputtering, spray painting [3], deposition of pesticides on plant leaves [4], etc. For most, if not all, of the applications, one wants to efficiently deposit a droplet, without spilling over any of the droplet material and without trapping air bubbles.

From a fundamental point of view, the last ten years have witnessed an enormous progress in the understanding of free-surface flows. In particular, the description of the surface singularities that are ubiquitous in these problems has greatly advanced [5]. Experimental and numerical studies have taken advantage of the recent progress in high-speed imaging techniques and computational power, respectively, to determine the self-similar behavior close to the singularities. Examples of much recent interest are drop formation [6–8], surface driven flows [9], and bubble collapse [10]. However, complete understanding of the drop impact problem remains nontrivial due to a complicated multiscale interplay between capillarity, viscous forces, inertia, and the properties of the solid surface [3,11].

In this Letter, we find that a surprising outcome of this interplay is that an ultrafine, high-speed jet can emerge from the drop, sending out part of the drop material elsewhere. In addition, for a certain range of impact velocities, the jet formation is accompanied by entrapment of air bubbles. Both the jet formation and the bubble entrapment are understood as a consequence of the formation of an air cavity that subsequently closes up in a singular (self-similar) fashion. We find that the cavity can close in two different ways, and, consequently, identify two distinct collapse singularities. A detailed analysis and theoretical interpretation of the singularities allow an understanding of

the main features of these high-speed and ultrathin emitted jets.

We study the impact of water droplets on a hydrophobic surface. The water drops (of density  $\rho = 1000 \text{ kg m}^{-3}$ , surface tension  $\gamma = 72 \text{ mN/m}$ ) are made using a precision needle which allows for a controlled release of spherical drop of radius  $R_1 = 1 \text{ mm}$ . The impact velocity  $V_{\text{impact}}$  of the droplets is varied simply by increasing the fall height. We use a superhydrophobic solid surface with a contact angle for water of  $\theta \sim 160^\circ$  [12]. The results described below are robust against viscosity changes (at least up to 10 times the water viscosity using water-glycerol mixtures), small variations of the drop radius or hydrophobicity: we obtain in fact very similar results for less hydrophobic, but still nonwetting surfaces (Parafilm and PDMS elastomer). However, due to contact line pinning on the solid, there is more scatter in the data; we will therefore restrict our discussion here to the superhydrophobic surfaces. Since the impact and subsequent jet formation are extremely rapid, we follow the drop impact using an ultra-high speed video system (Phantom V7), and use frame rates of 60 000 and 100 000 fps. Figure 1 depicts three series of snapshots of drops impacting at three different velocities (0.45, 0.56, and  $0.68 \text{ m} \cdot \text{s}^{-1}$ ). For all the cases studied here, the general dynamics of the impact consists in the spreading of the drop deformed by capillary waves followed by a retraction phase leading to the formation of a jet and finally to the total rebound of the droplet.

Since we use a low-viscosity liquid, viscous effects can be neglected in our experiments; the drop dynamics is therefore dictated by the Weber number  $We$ , which compares the inertial to the capillary forces,  $We = \rho R_1 V_{\text{impact}}^2 / \gamma$ . In the experiments  $We$  ranges between 0.6 and 16: this corresponds to small deformations on the scale of the droplets, as is indeed observed in the experiment. The jets, on the contrary, correspond to very large deformations, but have a very small characteristic size, Fig. 1.

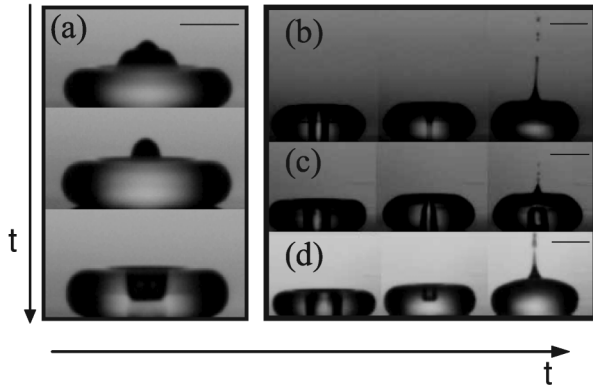


FIG. 1. Rapid camera snapshots. Impact of water drops (radius  $R_1 = 1$  mm) on a superhydrophobic surface. (a) Formation of the cylindrical air cavity: impact velocity  $V_{\text{impact}} = 0.45$  m  $\cdot$  s $^{-1}$ . Pictures taken 2.3, 2.7, and 3.4 ms after the impact time. (b)  $V_{\text{impact}} = 0.45$  m  $\cdot$  s $^{-1}$ . Pictures taken 3.8, 4.0, and 4.3 ms after the impact. (c) Impact velocity  $V_{\text{impact}} = 0.56$  m/s. Pictures taken 3.8, 4.2, and 4.4 ms after the impact. Note the presence of a trapped air bubble. (c) Impact velocity  $V_{\text{impact}} = 0.68$  m  $\cdot$  s $^{-1}$ . Pictures taken 3.7, 4.2, and 4.9 ms after the impact.

As the drop hits the surface, capillary waves are excited, propagate along the surface, and deform the drop into a pyramidal shape. The oscillations of the capillary waves then lead to the formation of a cylindrical air cavity located at the center of the drop along the vertical axis [Fig. 1(a)]. For the lowest impact speed, Fig. 1(b), the cavity retains its cylindrical shape all the way until its collapse. Conversely, for intermediate impact speeds, the bottom-up symmetry is broken almost immediately [see Fig. 1(c)]: the top of the cavity retracts faster than the bottom. As the liquid surface reconnects at the top, a bubble is entrapped. In Fig. 1(d), for higher impact speeds, the bottom of the cavity detaches itself from the solid surface prior to the cavity collapse, which leaves no bubble behind. By additionally filming some of the droplets from above, we determine whether dewetting due to the cavity formation occurs. We observe in fact rupture of the liquid film between the air cavity and the solid surface for  $0.37 < V_{\text{impact}} < 0.55$  m/s. The drop then adopts a toroidal shape. In all cases, the collapse of the air cavity is immediately followed by the violent ejection of a thin jet. For a low-viscosity fluid, the only intrinsic length scale in the problem is the wavelength of the capillary waves excited by the impact (i.e., the characteristic step size of the pyramidal drop). This length is on the order of  $\lambda \sim \gamma/(\rho V_{\text{impact}}^2)$  [13], an order of magnitude larger than the radius of the smallest jets.

We therefore need to understand the anomalously small size and large velocity of the jets. The velocity is determined by measuring the position of the top of the jet on four successive images when the jet emerges from the drop. We find that this velocity,  $V_{\text{jet}}$  can be 40 times larger than the impact speed:  $V_{\text{jet}} = 18$  m  $\cdot$  s $^{-1}$  for  $V_{\text{impact}} = 0.45$  m  $\cdot$  s $^{-1}$ . The variation of the jet speed,  $V_{\text{jet}}$ , and of the jet radius,  $R_{\text{jet}}$ , are nonmonotonic and highly nontrivial,

as shown in Fig. 2. We identify three main regions, separated by dotted lines and denoted I, II, and III.

*Region I.*—At small impact velocities, when increasing the impact velocity, the jet radius decreases rapidly whereas its velocity appears to diverge as the impact velocity approaches  $V_{\text{I-II}}$ . In parallel, the jet radius, measured just after its formation, becomes very small.

*Region II.*—This region corresponds to very small values of the jet radius and high jet velocities, and a rather complicated behavior of the jet velocity is observed as a function of  $V_{\text{impact}}$ . The latter is due to a subtle interplay between the rupture of the liquid film and entrapment of air bubbles. When approaching  $V_{\text{II-III}}$ , we observe bubble entrapment as shown in Fig. 1(b) for  $V_{\text{impact}} \geq 0.55$  m/s, as indicated by the black arrow in Fig. 2. The entrapment is clearly due to the closing of the drop top surface before the air can escape from the cavity, neither from the top before the cavity closes, nor through the bottom since the liquid film does not open [14]. Our experiment thus suggests that two conditions need to be fulfilled for entrapment: the cavity closes at the top and the air is not evacuated from the bottom.

*Region III.*—For “high” impact velocities a decrease in radius and a diverging jet velocity are found upon *decreasing* the impact velocity. As  $V_{\text{impact}} > V_{\text{II-III}}$  air bubbles are not trapped in the liquid anymore.

The high-speed movies (and Fig. 1) clearly show that the jet is formed due to the collapse of the air cavity. To understand what fixes the jet’s length and velocity scale, we thus need to consider the collapse dynamics in detail. This allows us to show that the jet structure with its anomalous length and velocity scales is fully determined by the collapse dynamics of the cavity.

The jets ejected for  $V_{\text{impact}}$  close to  $V_{\text{I-II}}$  result from the pinch-off singularity of an air cylinder immersed in a low viscosity liquid. Investigating the collapse dynamics in detail [between images 1 and 3 on Fig. 1(b)], we observe that the air thread exhibits self-similar behavior characteristic of a finite-time singularity, with a character-

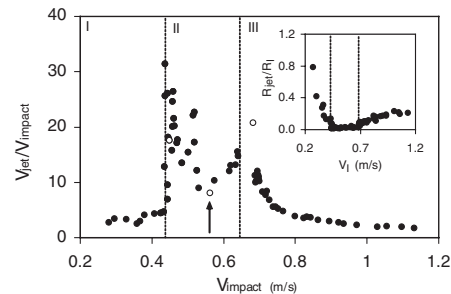


FIG. 2. The jet velocity normalized by the impact velocity is shown as a function of  $V_{\text{impact}}$ . The inset shows the jet radius. Three regions are identified separated by dotted lines at  $V_{\text{I-II}} = 0.45$  and  $V_{\text{II-III}} = 0.65$  ms $^{-1}$ . Open symbols correspond to the same experiments as in Figs. 1(a)–1(c). Inset: Jet radius normalized by the initial drop radius plotted versus the impact speed.

istic exponent for the vanishing of the cavity radius  $R = A(t_c - t)^{0.5 \pm 0.01}$ , with  $A = 0.02 \pm 0.003 \text{ m} \cdot \text{s}^{-1/2}$ , see Fig. 3. This dynamics is found almost but not completely up to the singularity point. Rather, very close to the singularity the air cylinder suddenly breaks down at some critical radius  $R_c$ . This loss of the cylindrical symmetry of the cavity depends in fact on the initial velocity  $V_{\text{impact}}$ . This is an incredibly rapid process: even when filming at 100 000 fps, the air cavity disappears in a single image.

Similar cylindrical pinch-off was described recently in bubble pinch-off in different liquids [15] and for cavity closure after impacts of steel balls on dilute granular materials [16]. For the latter, the pinch-off is followed by jet formation as is also the case here. For the former, a similar and equally surprising deviation from the self-similar behavior close to the singularity was reported. The pinch-off dynamics for all three cases is given by the Rayleigh-Plesset equation [6,17] for cylindrical free-surface flows. With the assumption that the air viscosity can be neglected it reads for an inviscid fluid:

$$\frac{P(r) - P_0}{\rho} = (\ddot{R}R + \dot{R}^2) \ln\left(\frac{R}{r}\right) + \frac{1}{2}\dot{R}^2 - \frac{\gamma}{\rho R}, \quad (1)$$

where  $P$  is the pressure,  $R(t)$  is the radius of the cavity, and  $r$  is a large-scale cutoff, on the order of the drop radius. For low-viscosity fluids, the pinch-off dynamics is dominated by inertia and the first term on the right-hand side. If indeed all other terms can be neglected, this implies that the prefactor of the logarithm is zero, leading immediately to  $R(t) \propto A(t_c - t)^{1/2}$  for the radius of the cylinder [18], in excellent agreement with the experimental data. In addition to the correct scaling, the prefactor  $A$  can be estimated using simple dimensional analysis:  $A \approx (\gamma R_1 / \rho)^{1/4}$ . This leads to  $A \approx 1.6 \times 10^{-2} \text{ m} \cdot \text{s}^{-1/2}$ , in good agreement with the experimental value.

We can now use our understanding of the cavity dynamics to account for the jet velocity. In Fig. 4 we show  $V_{\text{jet}}$  as a

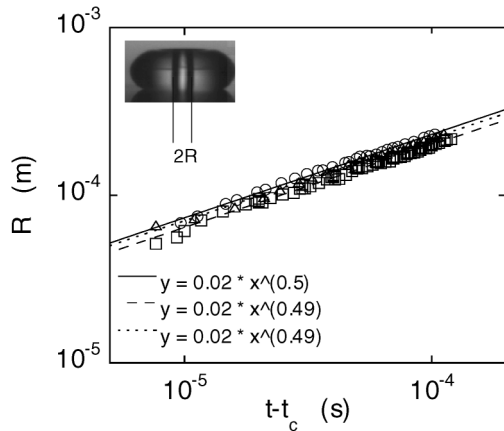


FIG. 3. Radius of the cylindrical cavity  $R$  plotted versus  $|t - t_c|$ . Triangles: drop impact speed  $V_{\text{impact}} = 0.43 \text{ m} \cdot \text{s}^{-1}$ . Circles:  $V_{\text{impact}} = 0.46 \text{ m} \cdot \text{s}^{-1}$ . Squares:  $V_{\text{impact}} = 0.52 \text{ m} \cdot \text{s}^{-1}$ . Lines: power law fits.

function of the radius of the air cavity at rupture  $R_c$  and similarly as a function of the jet radius  $R_{\text{jet}}$ . Clear power law relations over more than one decade of  $V_{\text{jet}}$  are observed:  $V_{\text{jet}} \propto (R_c/R_1)^{-1.9 \pm 0.2}$ , where  $R_c$  is the cavity radius just prior to the collapse, and  $V_{\text{jet}} \propto (R_{\text{jet}}/R_1)^{-0.9 \pm 0.2}$ .

To understand these relations between the jet velocity and radius on the one hand, and the critical cavity radius on the other hand, we propose a simple semiquantitative model based on mass and kinetic energy fluxes, neglecting both viscous and capillary effects. At the onset of cavity rupture, the pinch-off dynamics described above leads to a velocity of collapse of the air cylinder equal to  $\dot{R}(t) = A/[2(t_c - t)^{1/2}] = A^2/(2R_c)$ . Recalling that the bulk velocity field is steady for inertia dominated cylindrical collapse, we can use a balance equation through the boundary defined by the radius  $R_v$  and the height of the deformed drop, taken here to be on the order of the initial drop radius  $R_1$ . Then, mass conservation gives:  $[2\pi R(t)h]\dot{R}(t) = 2[\pi R_c^2]V_{\text{jet}}$ , and  $h \sim R_1$  which leads to

$$V_{\text{jet}} = \frac{A^2}{2R_1} \left(\frac{R_c}{R_1}\right)^{-2}. \quad (2)$$

The relation between the jet radius and the jet velocity can be inferred using a second conservation law. The continuity equation for the kinetic energy fluxes at the onset of the jet shooting reads:  $\frac{1}{2}\rho\dot{R}^3(t)[2\pi R(t)h] = 2\frac{1}{2}\rho V_{\text{jet}}^3[\pi R_{\text{jet}}^2]$ , using Eq. (2), we obtain

$$V_{\text{jet}} \approx \frac{A^2}{2R_1} \left(\frac{R_{\text{jet}}}{R_1}\right)^{-1}. \quad (3)$$

Equations (2) and (3) correctly predict the scaling relations between  $V_{\text{jet}}$ ,  $R_{\text{jet}}$ , and  $R_c$ :  $V_{\text{jet}} \propto (R_c/R_1)^{-2}$  and  $V_{\text{jet}} \propto (R_{\text{jet}}/R_1)^{-1}$ , in good agreement with the experimental data. These results are strongly substantiated by the complete absence of free fitting parameters, since  $A$  is known

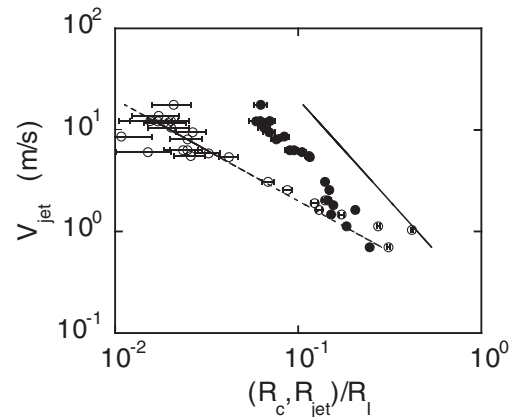


FIG. 4. Open circles: Jet velocity plotted versus the jet radius normalized by the initial drop radius,  $R_{\text{jet}}/R_1$ . Dashed line: theoretical prediction obtained from Eq. (2). Filled circles: Jet velocity plotted versus the cylindrical cavity radius before collapse normalized by the initial drop radius  $R_c/R_1$ . Full line: theoretical prediction obtained from Eq. (3).

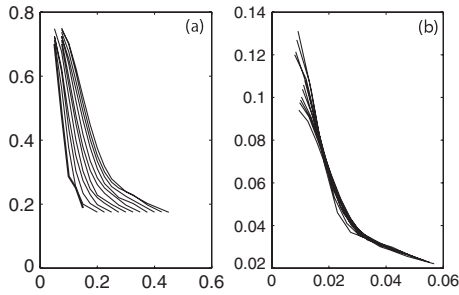


FIG. 5. Self-similar structure of the jet. Impact velocity:  $V_{\text{impact}} = 0.687 \text{ m} \cdot \text{s}^{-1}$ . Left: twelve superimposed jet profiles for different times (time interval  $15 \mu\text{s}$ ). First profile taken  $0.17 \text{ ms}$  after the collapse of the air bubble. Axes units: mm. Right: the same curves have been rescaled by a factor of  $(t - t_c)^{2/3}$  for the  $x$  and  $y$  coordinates, following the scaling behavior expected for self-similar dynamics in a capillary-inertial regime (arbitrary units for the rescaled profile plots).

from the void collapse dynamics. Figure 3 compares the theoretical predictions with the experimental results; given the simplicity of our model, the agreement with the experimental data is quite satisfactory not only for the scaling exponents but also for the numerical prefactors.

The last observation that needs to be explained is then the divergence of the jet velocity upon approaching  $V_{\text{II-III}}$ . Experimentally, the transition between regions II and III can also be identified by the topological change from a simply connected topology to a multiply connected topology, revealed by the bubble trapping. The divergence of the velocity and the topological change bear a striking similarity to the capillary-inertial singularities observed for driven Faraday waves [19] and for bubbles bursting at the free surface of a liquid [10]. For these two cases, the singular behavior can be accounted for by balancing capillary and inertial forces. It was shown, see, e.g., [19], that all length scales behave self-similarly as  $|t - t_c|^{2/3}$ , with  $t_c$  the collapse time. Our camera is not fast enough to follow the ultrafast collapse dynamics of the air cavity prior to the jet formation [Fig. 1(d)]. However, we did manage to monitor the shape of the jet profile for  $V_{\text{impact}}$  slightly above  $V_{\text{II-III}}$ , and, consequently, probe the dynamics after the singularity. Theoretically there is no reason why the length scales should not follow the same  $|t - t_c|^{2/3}$  behavior after the singularity. However, this post-singular regime has hardly ever been investigated in detail [20]. Figure 5 shows the rescaling of the different jet profiles taken at a regular time interval. The different profiles converge reasonably well onto a single master curve, in agreement with the idea that the dynamics after the singularity is still governed by capillary-inertial self-similar dynamics. The rather surprising conclusion is, therefore, that although the jet velocity diverges upon approaching both  $V_{\text{I-II}}$  and  $V_{\text{II-III}}$ , the underlying collapse singularities leading to the jet divergence is fundamentally different in the two cases.

In summary, we have shown here that gentle drop impacts can lead to singular behavior. The most surprising

features of this are the anomalously small lengths and high velocities: very narrow jets are formed that shoot out with speeds up to 40 times the drop impact velocity. As is the case for all singular jets in liquids, granular media, for Faraday waves, etc., the jet formation is preceded by the collapse of an air cavity. It is this singularity that is responsible for the selection of the anomalous length and velocity scales of the jets. We have related here, for the first time, the collapse dynamics of the cavity to the divergence of the speed of the jet. An open question remains what intrinsic length scale provides the cutoff mechanism for the singularity. In our experiment, close to  $V_{\text{I-II}}$  the maximum velocity of the jet is bound by the minimum radius the cavity can reach. This turns out to be rather different from a microscopic length scale: the cylindrical cavity destabilizes at  $\approx 50 \mu\text{m}$ , the reason for which remains unclear.

\*denis.bartolo@lps.ens.fr

†josserand@imm.jussieu.fr

‡daniel.bonn@lps.ens.fr

- [1] A. Worthington, Proc. R. Soc. London **25**, 261 (1876).
- [2] D. B. Dam and C. Le Clerc, Phys. Fluids **16**, 3403 (2004).
- [3] R. Rioboo, M. Marengo, and C. Tropea, Atomization and Sprays **11**, 155 (2001).
- [4] V. Bergeron, D. Bonn, J.-Y. Martin, and L. Vovelle, Nature (London) **405**, 772 (2000).
- [5] J. Eggers, Rev. Mod. Phys. **69**, 865 (1997).
- [6] A. Prosperetti and H. N. Oguz, Annu. Rev. Fluid Mech. **25**, 577 (1993).
- [7] I. Cohen, M. P. Brenner, J. Eggers, and S. R. Nagel, Phys. Rev. Lett. **83**, 1147 (1999).
- [8] R. F. Day, E. J. Hinch, and J. R. Lister, Phys. Rev. Lett. **80**, 704 (1998).
- [9] J. Keller and M. Miksis, SIAM J. Appl. Math. **43**, 268 (1983).
- [10] L. Duchemin, S. Popinet, C. Josserand, and S. Zaleski, Phys. Fluids **14**, 300 (2002).
- [11] M. Rein, Fluid Dyn. Res. **12**, 61 (1993).
- [12] F. Bouamrine (private communication).
- [13] Y. Renardy *et al.*, J. Fluid Mech. **484**, 69 (2003).
- [14] This is very different from the bubble formation considered in Mehdi-Nejad *et al.*, where the bubble is entrapped in a very early stage of the impact due to the drop deformation. V. Mehdi-Nejad, J. Mostaghimi, and S. Chandra, Phys. Fluids **15**, 173 (2003).
- [15] J. C. Burton, R. Waldrep, and P. Taborek, Phys. Rev. Lett. **94**, 184502 (2005).
- [16] D. Lohse, R. Bergmann, R. Mikkelsen, C. Zeilstra, R. van der Meer, M. Versluis, J. van der Weele, M. van der Hoef, and H. Kuipers, Phys. Rev. Lett. **93**, 198003 (2004).
- [17] M. S. Plesset and A. Prosperetti, Annu. Rev. Fluid Mech. **9**, 145 (1977).
- [18] This scaling is valid up to logarithmic corrections; see J. M. Gordillo *et al.*, Phys. Rev. Lett. **95**, 194501 (2005).
- [19] B. Zeff, B. Kleber, J. Fineberg, and D. Lathrop, Nature (London) **403**, 401 (2000).
- [20] J. E. Hogrefe, Physica D (Amsterdam) **123**, 183 (1998).